The *Caenorhabditis elegans spe-5* Gene Is Required for Morphogenesis of a Sperm-Specific Organelle and Is Associated With an Inherent Cold-Sensitive Phenotype

Khaled Machaca[1] and Steven W. L'Hernault

Graduate Division of Biological and Biomedical Sciences, and Department of Biology, Emory University, Atlanta, Georgia 30322

Manuscript received September 6, 1996
Accepted for publication March 11, 1997

ABSTRACT

The nonrandom segregation of organelles to the appropriate compartment during asymmetric cellular division is observed in many developing systems. *Caenorhabditis elegans* spermatogenesis is an excellent system to address this issue genetically. The proper progression of spermatogenesis requires specialized intracellular organelles, the fibrous body-membranous organelle complexes (FB-MOs). The FB-MOs play a critical role in cytoplasmic partitioning during the asymmetric cellular division associated with sperm meiosis II. Here we show that *spe-5* mutants contain defective, vacuolated FB-MOs and usually arrest spermatogenesis at the spermatocyte stage. Occasionally, *spe-5* mutants containing defective FB-MOs will form spermatids that are capable of differentiating into functional spermatozoa. These *spe-5* spermatids exhibit an incomplete penetrance for tubulin mis-segregation during the second meiotic division. In addition to morphological and FB-MO segregation defects, all six *spe-5* mutants are cold-sensitive, exhibiting a more penetrant sterile phenotype at 16° than 25°. This cold sensitivity could be an inherent property of FB-MO morphogenesis.

AN important requirement for proper cellular differentiation is the correct temporal and spatial positioning of gene products and organelles. Cellular polarization is observed in many cell types and has been extensively studied in, for instance, the targeting of membrane proteins within cultured epithelial cells (EATON and SIMONS 1995; MOSTOV and CARDONE 1995) or segregation of organelles to the *Saccharomyces cerevisiae* bud (DRUBIN 1991). Understanding the regulation and machinery involved in this cellular polarization is, therefore, crucial. Segregation of both cellular organelles and macromolecular structures is a prominent feature of *Caenorhabditis elegans* spermatogenesis. Many mutations that affect these segregation processes are available, making this system especially attractive for detailed analyses (reviewed by L'HERNAULT 1997).

Wild-type *C. elegans* spermatogenesis has been reviewed elsewhere (L'HERNAULT 1997) but is briefly summarized below. Spermatogenesis is a linear differentiation pathway where mitotic spermatogonial stem cells at the distal end of the gonad ultimately become polar, amoeboid spermatozoa capable of fertilization (HIRSH *et al.* 1976; KLASS *et al.* 1976; WOLF *et al.* 1978; WARD *et al.* 1981). Spermatogonial cells become spermatocytes while in a syncytium with a central cytoplasmic core called the rachis (Figure 3Aa). Syncitial primary spermatocytes initiate meiosis, bud off the rachis as distinct cells at the proximal end of the gonad (Figure 3Ab) and complete the first meiotic division; this first meiotic division may or may not be coupled to cytokinesis (Figure 3Ac). The second meiotic division results in four haploid spermatids and one or two residual bodies (Figure 3Ad). The second division is asymmetric, and nuclei, centrosome, fibrous body-membranous organelle complexes (FB-MO; see below), and mitochondria segregate to spermatids (Figure 3Ae) as they separate from a residual body that contains ribosomes, actin and noncentrosomal tubulin (WARD 1986).

The FB-MO complexes transport materials required for spermatids to differentiate into spermatozoa (Figure 8A; ROBERTS *et al.* 1986). MO first appear in meiotic cells (as in Figure 3Aa) that are still in syncytium with the rachis (Figure 8Aa). The FB first appears as short fibers of major sperm protein (MSP; KLASS and HIRSH 1981) in the body of the MO (Figure 8Aa) that increase in size as sperm cells develop. The mature FB is partially enclosed within a double layered membrane in the MO (Figure 8Ab). The FB-MOs segregate into spermatids after the second meiotic division. At the budding spermatid stage, the double layered membrane surrounding the FB retracts, and the MSP fibers disassemble into MSP dimers (Figure 8Ac; KLASS and HIRSH 1981; ROBERTS *et al.* 1986). After the FB disappears, the MOs are located beneath the spermatid plasma membrane (Figure 8Ad). The MO head fuses with the plasma membrane during conversion of spermatids

Corresponding author: Steven W. L'Hernault, Department of Biology, Emory University, 1510 Clifton Rd., Atlanta, GA 30322.
E-mail: bioslh@biology.emory.edu

[1]*Present address:* Department of Anatomy and Cell Biology, Emory University School of Medicine, Atlanta, GA 30322.

into spermatozoa, releasing a glycoprotein calyx onto the cell surface (WARD *et al.* 1983). The collar lies beneath a permanent fusion pore in the spermatozoan plasma membrane that exposes the MO interior to the extracellular environment (Figure 8Ae). MSP dimers reassemble into fibers within the pseudopod, where they play a role in sperm amoeboid motility (ROBERTS *et al.* 1986).

A number of spermatogenesis defective (*spe*) mutants alter FB-MO morphogenesis (reviewed by L'HERNAULT 1997). An interesting example is *spe-4*, which arrests spermatogenesis at the spermatocyte stage. The resulting terminal spermatocytes have four haploid nuclei but are incapable of completing cytokinesis (L'HERNAULT *et al.* 1988). *spe-4* encodes an integral membrane protein (L'HERNAULT and ARDUENGO 1992), with homology to the presenilin family of proteins that are associated with early onset familial Alzheimer's disease (LEVY-LAHAD *et al.* 1995; ROGAEV *et al.* 1995; SHERRINGTON *et al.* 1995).

This paper describes *spe-5* mutants, which arrest spermatogenesis at the primary spermatocyte stage in a manner reminiscent of *spe-4* (L'HERNAULT *et al.* 1988; L'HERNAULT and ARDUENGO 1992). These studies reveal that the *spe-5* gene product is required for proper FB-MO morphogenesis during *C. elegans* spermatogenesis. Additionally, *spe-5* mutants exhibit other pleiotropic defects, including multiple DAPI positive regions and unusual tubulin localization. Lastly, all six *spe-5* alleles are cold-sensitive, suggesting an inherent temperature sensitivity of FB-MO morphogenesis.

MATERIALS AND METHODS

Strains and genetic analysis: *C. elegans* var. Bristol (N2) was the wild-type strain used in this work. The following genes and mutations were used in this study: *spe-5(hc93), (hc110), (oz3), (oz46), (eb29),* and *(eb30) I; dpy-5(e61) I; unc-13(e51) I; dpy-14(e188) I* (BRENNER 1974); *mes-3(bn21ts) I* (PAULSEN *et al.* 1995); *unc-38(x20) I* (LEWIS *et al.* 1980); and *him-5(e1490) V* (HODGKIN *et al.* 1979). The chromosome I duplications *sDp2* (HOWELL *et al.* 1987), *hDp20, hDp22, hDp29* (MCKIM and ROSE 1990) and the deficiency *sDf4* (ROSE 1980) were also employed. The isolation and preliminary characterization of the *spe-5* alleles *hc93* and *hc110* have been described previously (L'HERNAULT *et al.* 1988). *spe-5(oz46)* and *spe-5(oz3)* both arose in F_2 screens for females. *spe-5(oz46)* is EMS-induced and *spe-5(oz3)* arose spontaneously in a *mut-3* strain (COLLINS *et al.* 1987); both were kindly provided by T. SCHEDL (Washington University School of Medicine, St. Louis, MO). *spe-5(eb29)* and *spe-5(eb30)* are EMS-induced mutations and were isolated by P. M. ARDUENGO during an F_1 noncomplementation screen for new *spe-5* and *spe-4* alleles over a *spe-5(hc93) dpy-5(e61) unc-13(e51) spe-4(q347)* chromosome. The free duplication *sDp2* (HOWELL *et al.* 1987) was used to balance *spe-5*, and the noncomplementing deficiency *sDf4* (ROSE 1980; L'HERNAULT *et al.* 1988) was employed to generate hemizygous *spe-5* animals. Phenotypic characterization of all six *spe-5* mutants was performed in a *dpy-5(e61); him-5(e1490)* mutant background. The *dpy-5(e61)* mutation was used as a tightly linked *cis*-morphological marker to easily identify *spe-5* mutant animals, and the *him-5* mutation was used to increase the incidence of males

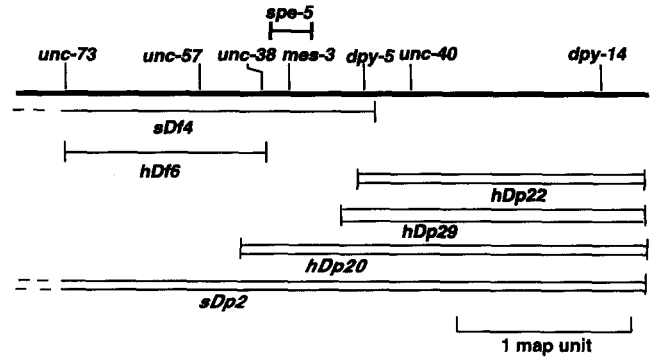

FIGURE 1.—A partial genetic map of the left arm of chromosome I. The thick bar represents the chromosome, and the genetic positions of morphological and other markers are indicated by a vertical line. Duplications (*Dp*) are drawn as a double line and deficiencies (*Df*) as a single line. The region containing *spe-5*, as deduced from data discussed in MATERIALS AND METHODS and L'HERNAULT *et al.* (1988), is indicated above the chromosome.

(HODGKIN *et al.* 1979). The use of *dpy-5* as a tightly linked marker was essential because the *spe-5*-associated sterile phenotype was not completely penetrant. The *dpy-5; him-5* or *dpy-5* genetic backgrounds were controls for all experiments, and neither gene has any obvious effect on sperm differentiation (WARD *et al.* 1983; L'HERNAULT *et al.* 1988).

The *spe-5* gene was mapped relative to the *hDp20, hDp22,* and *hDp29* duplications and the *unc-38, mes-3* and *dpy-5* genes (Figure 1). All tested duplications cover (include) the *dpy-5* gene. Duplication mapping was performed by generating *Dp/spe-5 (hc93) dpy-5/spe-5 (hc93) dpy-5* non-Dpy hermaphrodites and scoring their self-fertility at 20°. This analysis shows that *hDp20* covers (and balances), while *hDp22* and *hDp29* do not cover *spe-5*. From *spe-5(hc110)/unc-38(x20) dpy-5(e61)* hermaphrodites five of 10 Dpy non-Unc and four of eight Unc non-Dpy recombinants were *spe-5/+*. This indicates that *spe-5* is located between *unc-38* and *dpy-5* and suggests it is about equidistant from these markers. From *mes-3(bn21ts)/spe-5(hc93) dpy-5(e61),* 25 Dpy non-Spe hermaphrodites were scored and all proved to be Mes, which suggests that *spe-5* is right of and close to *mes-3* or left of *mes-3*. The duplication and deficiency complementation pattern of *spe-5* and *mes-3* are identical, so the available information is insufficient to order *spe-5* with respect to *mes-3*. Two lethal genes, *let-359* and *let-364*, are located in this region of chromosome I (MCKIM and ROSE 1990) and both complement *spe-5(hc93)* so that heterozygotes are non-Spe and non-Let (not shown).

Light microscopy: Virgin L4 *dpy-5; him-5* control or *spe-5 dpy-5; him-5* males were placed on agar plates without hermaphrodites for 2–5 days at 16°. All of the *spe-5*-associated phenotypes are observed in young (newly molted adults) as well as males aged to allow accumulation of cells formed during spermatogenesis. None of the described defects were ever observed in control *dpy-5* males, irrespective of their age. This ensured that the necrotic-like phenotypic effects of *spe-5* on spermatogenesis are not due to overly aged cells. Sperm development and morphology were observed under differential interference contrast (DIC) optics after hand dissection of males in a drop of sperm medium (SM; L'HERNAULT and ROBERTS 1995). The composition of SM was as follows: 5 mM Hepes, 50 mM NaCl, 25 mM KCl, 5 mM $CaCl_2$, 1 mM $MgSO_4$, pH 7.0. The osmolarity was equilibrated to 230 mOsm with dextrose (MACHACA *et al.* 1996). Nuclear morphology was examined in worms dissected in SM containing 1 μg/ml of 4,6-diamidino-2-phenylindole (DAPI) (Sigma, St. Louis, MO),

and fluorescently stained nuclei were observed under epi-illumination. For other types of cytological analyses, cells were fixed and stained with DAPI as described below.

Immunocytolocalization: Immunocytochemistry was carried out as described in VARKEY *et al.* (1993) with minor modifications. Males were dissected in a 5 μl drop of SM on a slide freshly coated with poly-lysine, and incubated for 10–20 min in a humid chamber to permit settling and attachment of cells. The cells were overlaid with 200 μl of 4% paraformaldehyde in SM for 30 min. A cover slip was placed on top of the sample, and the slide was frozen on a block of dry ice while applying gentle pressure to the cover slip. After 5 min, the cover slip was removed from the frozen sample. The cells were rinsed three times in PBS for 5 min each, and then five times for 5 min each in PBS containing 10 mg/ml glycine to block unreacted aldehydes. The cells were permeabilized in PBS containing 5% Triton X-100 for 5 min, briefly rinsed with PBS, and incubated for 15 min with PBS containing 5% goat serum. After a brief wash in PBS, the sample was incubated with primary antibody or rhodamine-conjugated phalloidin (see below), rinsed with PBS, rinsed again with PBS containing 5% goat serum, and incubated for another 30 min with fluorescently conjugated secondary antibodies when appropriate. Following incubation with secondary antibodies, samples were rinsed three times for 5 minutes each in PBS and then incubated in PBS containing 40 ng/ml DAPI for 10 min. The samples were mounted in 1,4-diazabicyclo-[2.2.2] octane (DABCO) (Sigma, St. Louis, MO) saturated Aquamount (Lerner, Pittsburgh, PA), coverslipped and sealed with nail polish. The slides were viewed by epi-fluorescence through appropriate filters.

The monoclonal antibody 1CB4 was raised against total worm homogenates and it recognizes chemosensory neurons, intestine and sperm (OKAMOTO and THOMSON 1985). In sperm, 1CB4 specifically stains the MOs (OKAMOTO and THOMSON 1985). 1CB4 hybridoma culture supernatant was used at 1:100 dilution. The anti-α-tubulin monoclonal antibody (B-5-1-2) was provided by W. SALE (SALE *et al.* 1988) and was used at a 1:20 dilution. An 80-μM stock solution of phalloidin conjugated to FITC was prepared according to the manufacturer's recommendation (Sigma, St. Louis, MO) and was diluted to 0.4 μM for use in actin staining experiments. The anti-MSP polyclonal serum (sw3) was a generous gift from S. WARD and was used at 1:500 dilution (BURKE and WARD 1983). Fluorescently tagged, affinity-purified secondary antibodies were goat anti-mouse TRITC labeled IgG used at 1:1000 dilution (Jackson Laboratories, West Grove, PA), and goat anti-rabbit TRITC labeled IgG used at 1:500 dilution (Boehringer Mannheim, Indianapolis, IN).

Electron microscopy: Sperm cells were prepared for EM analysis essentially as described by SHAKES and WARD (1989), except that the samples were embedded in LX112 (Ladd Research Industries Inc., Burlington, VA).

RESULTS

***spe-5* genetics and isolation of new alleles:** The *spe-5* gene is defined by a total of six alleles. Two *spe-5* alleles (*hc93* and *hc110*) have been described in a previous publication (L'HERNAULT *et al.* 1988). Two new *spe-5* alleles (*oz3* and *oz46*) were recovered as Spe animals in F_2 genome wide screens for females (T. SCHEDL, personal communication). The other two *spe-5* alleles (*eb29* and *eb30*) were recovered in an F_1 noncomplementation screen (see MATERIALS AND METHODS). All six mutants exhibit defective spermatogenesis and lay oocytes on the growth plate, which are typical defects for Spe mutants (see below). We have detected no effects on growth or morphogenesis of any somatic tissues in these mutants (data not shown).

***spe-5* associated cold sensitivity:** The brood sizes of *dpy-5* control hermaphrodites were lower at 25° than at 16°, as is the case for wild-type animals (*e.g.*, L'HERNAULT *et al.* 1988). This temperature-sensitive effect on self-fertility is due to lower sperm production at 25° than at 16°, and is also a characteristic of wild-type hermaphrodites (HIRSH *et al.* 1976). In contrast, the brood sizes of *spe-5 dpy-5* mutant animals were found to exhibit incomplete penetrance associated with a cold-sensitive enhancement of self-sterility (Figure 2). At 25°, the majority of *spe-5* mutant hermaphrodites lay oocytes and produce no progeny (Figure 2A). However, some hermaphrodites produce a few self-progeny (<20), while others have brood sizes similar to the *dpy-5* control hermaphrodites. Analyses were performed on *spe-5 dpy-5* mutant hermaphrodites picked from *sDp2/spe-5 dpy-5* balanced lines based on their Dumpy (Dpy) phenotype. This strategy should reliably identify *cis spe-5 dpy-5* double mutants because *sDp2* is an excellent balancer and crossover suppressor (ROSE *et al.* 1984; HOWELL *et al.* 1987). However, the self-fertility exhibited by certain 25°-raised Dpy hermaphrodites segregated from these balanced strains could be due, in principle, to recombination between *dpy-5* and *spe-5*. Consequently, 12 L4 progeny were picked from each putative *spe-5 dpy-5* hermaphrodite that produced >20 progeny and their brood sizes were determined. Most hermaphrodites from these broods were self-sterile and nearly all remaining hermaphrodites produced only a few progeny, indicating that recombination between *spe-5* and *dpy-5* had not occurred. Additional attempts to isolate *spe-5* homozygotes that consistently segregated self-fertile progeny at 25° also proved unsuccessful (not shown). While most hermaphrodites of any *spe-5* genotype are self-sterile when they are raised at 16°, self-fertile individuals are also observed at this growth temperature (Figure 2B). The number of self-fertile Spe-5 individuals and the average brood size of those individuals are both lower at 16° than at the 25° growth temperature, indicating that the self-sterile *spe-5* phenotype is cold-sensitive. The magnitude of this temperature effect on self-fertility varies among the *spe-5* mutants. The mean self-fertility exhibited by the *spe-5(oz3)* mutant is least affected, and it is less than twofold lower at 16° than it is at 25°. At both temperatures, this mutant has an average brood size of less than two progeny per hermaphrodite. In contrast, the mean brood size of *spe-5(eb30)* is ~45-fold lower at 16° than it is at 25°, and it is the least penetrant mutant at 25° but nearly completely self-sterile at 16°.

The above data establish that *spe-5* exhibits a phenotype that appears to be intrinsically cold-sensitive. Consequently, the strongest mutant at 16° (the restrictive

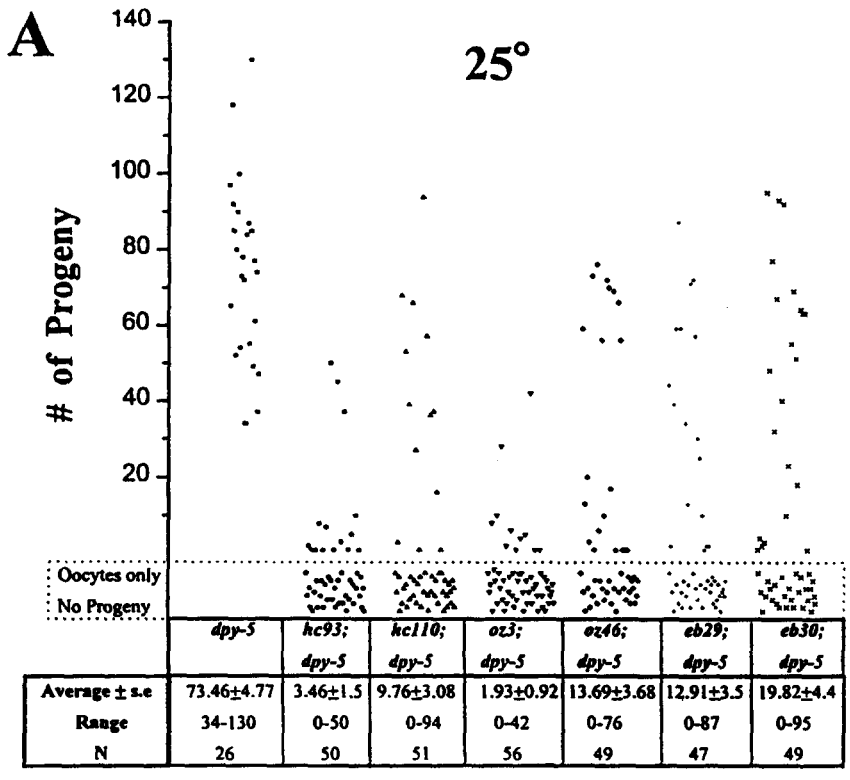

	dpy-5	hc93; dpy-5	hc110; dpy-5	oz3; dpy-5	oz46; dpy-5	eb29; dpy-5	eb30; dpy-5
Average ± s.e	73.46±4.77	3.46±1.5	9.76±3.08	1.93±0.92	13.69±3.68	12.91±3.5	19.82±4.4
Range	34-130	0-50	0-94	0-42	0-76	0-87	0-95
N	26	50	51	56	49	47	49

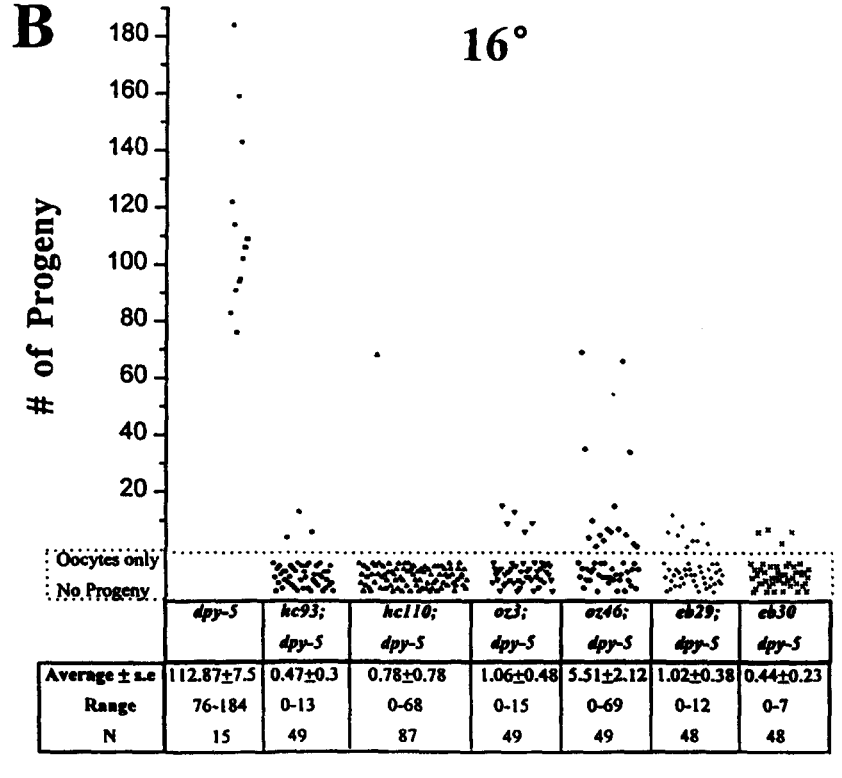

	dpy-5	hc93; dpy-5	hc110; dpy-5	oz3; dpy-5	oz46; dpy-5	eb29; dpy-5	eb30 dpy-5
Average ± s.e	112.87±7.5	0.47±0.3	0.78±0.78	1.06±0.48	5.51±2.12	1.02±0.38	0.44±0.23
Range	76-184	0-13	0-68	0-15	0-69	0-12	0-7
N	15	49	87	49	49	48	48

FIGURE 2.—*spe-5*-associated cold sensitivity. Hermaphrodites of the indicated genotype were picked individually as L4 larvae and their broods quantified over their life span, at both 25° (A) and 16° (B) growth temperatures. The number of progeny composing each hermaphrodite's brood is indicated on the *y*-axis. Each symbol on the graph represent the brood size of a single hermaphrodite. The symbols within the dashed box represent animals that laid only oocytes and produced no progeny. The non-Spe control for these experiments was *dpy-5(e61)* hermaphrodites, since all of the *spe-5* mutations tested were in *cis* to this marker. The *spe-5* allele tested is indicated below each data set, followed by the mean brood size ± SE, the range of brood sizes observed, and the number of animals tested (*N*).

temperature) should exhibit the strongest loss of function. However, the extent of self-fertility cannot be straightforwardly applied to order *spe-5* mutant hermaphrodites into an allelic series. The *spe-5(oz46)* mutant seems to be the weakest, producing a mean brood size that is approximately fivefold larger than *spe-5(oz3)*, which is the next most fecund mutant. Except for *spe-5(oz46)*, the other four mutants all exhibit a mean self-fertility that is similar. The *spe-5(hc110)* mutant is perhaps the best candidate for the strongest loss of function, based on the fact that it almost never produces any progeny when raised at 16°. However, the single, rare *spe-5(hc110)* hermaphrodite that exhibited self-fertility when raised at 16° produced a brood of 68 prog-

eny. Hemizygous *spe-5(hc110)/sDf4* hermaphrodites were examined at 16° and all six hermaphrodites proved completely self-sterile. However, *spe-5(hc110)* homozygotes only produce progeny rarely when reared at 16°, so it is possible that the *spe-5* null phenotype is intrinsically leaky. If this is so, then *spe-5(hc110)* is the best candidate for a null allele, based on the rarity of any self-fertile hermaphrodites.

***spe-5* light microscopic and nuclear phenotype:** The effects of *spe-5* on spermatogenesis in males were determined by a variety of light and electron microscopic techniques. For clarity, a cartoon summary of these data appears in Figure 3B, before presentation of the original data. The control for all *spe-5* phenotypic analyses was *dpy-5; him-5* males (Figure 4, A–H), and spermatogenesis in these males is indistinguishable from wild-type (WARD *et al.* 1981; L'HERNAULT *et al.* 1988). Primary spermatocytes that bud off the rachis (Figure 4A) contain a 4N nucleus (Figure 4E) that divides into two diploid nuclei (Figure 4F) in secondary spermatocytes (Figure 4B). During the second meiotic division, spermatids contain single haploid nuclei (Figure 4G), and start to bud away from the residual body (Figure 4C). After completion of the budding process, spermatids are separated from the residual body (Figure 4D) and are still characterized by condensed nuclei (Figure 4H). The cells were prepared by dissection of *dpy-5(e61); him-5(e1490)* control males that have been aged for 2–4 days at 16°. Under these conditions, the majority of wild-type cells are spermatids, since males store their sperm as spermatids in the vas deferens until mating (reviewed by L'HERNAULT 1997). In contrast, when *spe-5(hc110) dpy-5(e61); him-5(e1490)* males are prepared in the same fashion, a few spermatids are observed, but the majority of cells are terminally arrested, aberrant spermatocytes (Figure 4, I–R). Unlike controls (*e.g.*, Figure 4, A or B), *spe-5* aberrant spermatocytes usually exhibit a cratered appearance, apparently due to cytoplasmic vacuoles (*e.g.*, Figure 4, K and L). The total number of cells observed appears substantially lower than in control males (not shown). The majority of the arrested *spe-5* aberrant spermatocytes have lost their usually characteristic appearance (compare Figure 4, A, B or C to Figure 4, J, K or L). These aberrant spermatocytes usually contained four condensed nuclei, indicating that the meiotic nuclear divisions were completed (Figure 4O). Such aberrant spermatocytes apparently can progress to a stage that is similar to wild-type spermatid budding (as in Figures 3Ae and 4C), and condensed nuclei can reside in either bud-like structures or elsewhere at the periphery of the cell. The terminal spermatocyte shown in Figure 4J is attempting to form two buds, one is in the plane of focus and the other slightly out of focus. Two of the four nuclei (Figure 4O) in this cell are in these buds and the other two are at the opposite edge of the cell. In other instances, the budding process is more successful. The cell shown in Figure 4L, for example, has initiated the budding process with three apparent buds in this plane of focus. The characteristic vacuoles seen in *spe-5* cells, which give the cells a cratered appearance, usually segregate to the buds, and they surround a smooth area in the middle of the cell that is presumably the forming residual body (Figure 4L). The condensed nuclei reside in the forming buds (Figure 4Q). Some of the *spe-5* spermatocytes complete the budding process and generate spermatids (Figure 4M). These spermatids usually have a vacuolated appearance (Figure 4M), and the degree

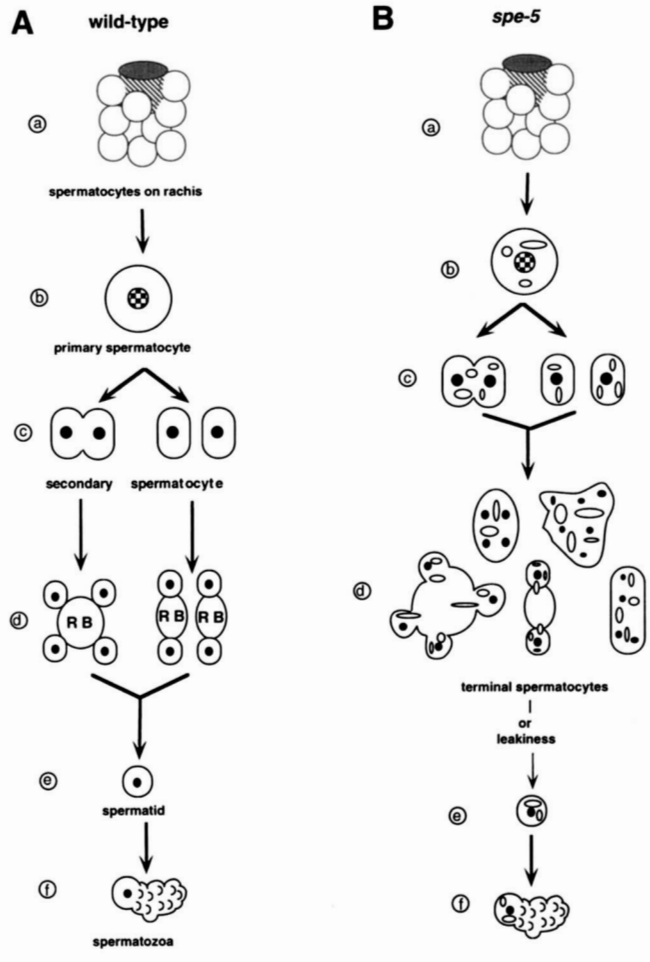

FIGURE 3.—Cartoon summary of wild-type spermatogenesis (A) and various defects observed in a *spe-5* mutant background (B). For both wild-type and *spe-5* mutants, spermatogenesis begins with spermatocytes in syncytium with a central cytoplasmic core named the rachis (hatched area in 3Aa and 3Ba). Primary spermatocytes bud from the rachis in wild-type (Ab) and *spe-5* mutants (Bb). At this point, vacuoles (open ovals) are evident in *spe-5* spermatocytes, and they are never observed in wild-type spermatocytes. These vacuoles are evident throughout the remaining stages of spermatogenesis in *spe-5* mutants. Secondary spermatocytes (Ac) divide (Ad) to yield spermatids (Ae) that differentiate into spermatozoa (Af) in wild type. Spermatids are only occasionally observed in *spe-5* mutants (Be), and some of these can differentiate into spermatozoa (Bf). More commonly, *spe-5* mutants arrest spermatogenesis while attempting the second cell division that accompanies meiosis II (Bd). RB refers to the residual body.

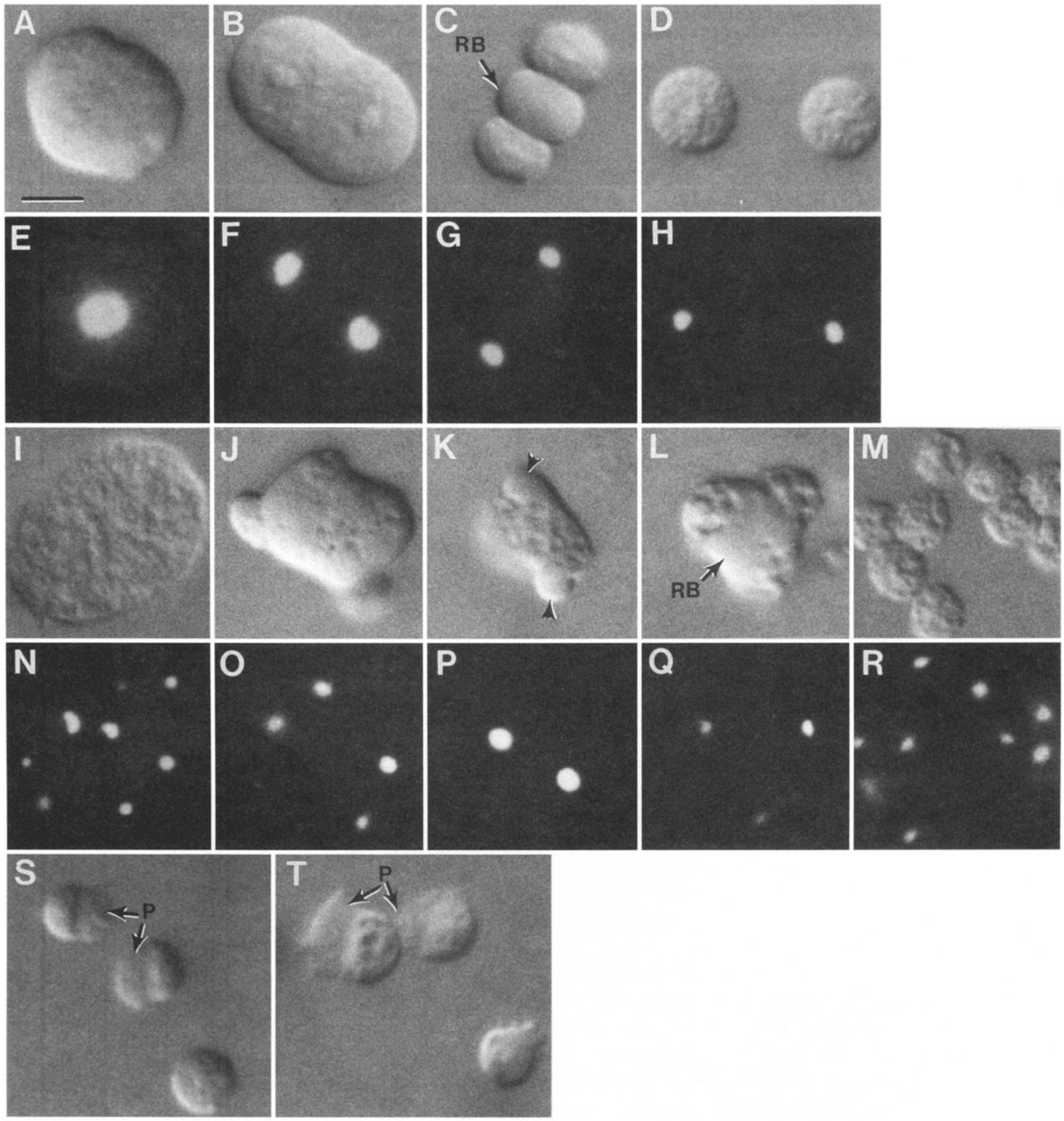

FIGURE 4.—Nuclear and light microscopic phenotype of wild-type and *spe-5* cells. Differential interference contrast images of wild-type (A–D) and *spe-5* (I–M) appear in the row over the corresponding DAPI images of nuclei. (E–H) DAPI stained *dpy-5(e61); him-5(e1490)* control cells. The 4N nucleus in the primary spermatocyte (A and E) becomes two diploid nuclei in secondary spermatocytes (B and F). At the budding spermatid stage (C and G) the nuclei are condensed, and remain that way in budded spermatids (D and H). RB refers to the residual body. (N–R) DAPI-stained *spe-5(hc110) dpy-5(e61); him-5(e1490)* cells. A variety of arrested terminal spermatocytes are shown (I–K) with their corresponding DAPI phenotype (N–P, respectively). L and Q show a *spe-5* spermatocyte at the budding spermatid stage, and M and R show *spe-5* spermatids. RB refers to the residual body, and arrow heads point to the residual body-like blebs in some *spe-5* terminal spermatocytes (see the text for more details). (S–T) *dpy-5(e61); him-5(e1490)* (S) or *spe-5(hc110) dpy-5(e61); him-5(e1490)* (T) spermatozoa activated in SM with 200 μg/ml Pronase are shown. Note the vacuoles (which appear as small craters) characteristic of *spe-5* cells in the left most spermatozoon in T. The arrows at P point to pseudopods on spermatozoa. All cells were prepared by hand dissection of virgin males that have been picked as L4s and aged without hermaphrodites for 2–4 days at 16°. Scale bar in A = 5 μm for A–T.

of vacuolation can vary (not shown). The nuclear phenotype of the rare *spe-5* spermatids appears normal (Figure 4R).

spe-5 terminal spermatocytes exhibit a complex array of aberrant morphological and nuclear phenotypes. Some cells show multiple DAPI-stained regions of differ-

ent intensity. For example, the terminal spermatocyte shown in Figure 4I has eight DAPI positive regions (Figure 4N) that are scattered throughout the cell. Cells with up to 18 DAPI staining spots were also observed (not shown). Another unusual variation on the *spe-5* terminal spermatocyte phenotype can be seen in the cell shown in Figure 4, K and P. This cell is apparently attempting to bud, but these buds are smooth (arrows in Figure 4K), like residual bodies (*e.g.*, Figure 4, C or L), and the cratered vacuoles are in the center of the cell. The nuclei are in the central region of the cell, which also contains the vacuoles, and not in the bud-like structures (compare Figure 4, K and P).

Functional spermatozoa must occasionally be produced by *spe-5(hc110) dpy-5* mutants raised at 16° because they can exhibit self-fertility (Figure 2B). Such rare *spe-5(hc110)* spermatids were observed (as in Figure 4M), and they were tested for their ability to differentiate into spermatozoa. Spermatozoa will form after wild-type spermatids are activated with Pronase (WARD *et al.* 1983), and this protease was tested for its effects on both *spe-5 dpy-5* and *dpy-5* control spermatids. *spe-5 dpy-5; him-5* spermatids activate into spermatozoa (Figure 4T) and their pseudopods have a similar morphology to *dpy-5; him-5* control cells activated in the same fashion (Figure 4S). However, these *spe-5* spermatozoa (Figure 4T) are not normal because crater-like vacuoles are visible in their cell body cytoplasm, which is also characteristic of terminally arrested *spe-5* spermatocytes (Figure 4, K and L) and *spe-5* spermatids (Figure 4M).

All of the cytological analyses presented above were performed on *spe-5(hc110)* mutants raised at 16° because they have the most uniform sterile phenotype under these conditions (Figure 2B). The nuclear and other cytological phenotypes of *spe-5(hc110)/sDf4* sperm were similar to that of *spe-5(hc110)* homozygous cells, suggesting that this represents the null phenotype of *spe-5* (data not shown). The cytological and nuclear phenotypes of the other five *spe-5* mutants were also examined in animals raised at 16°, and all mutants exhibited cytological and nuclear defects that were qualitatively similar to *spe-5(hc110)*. Although some variation was observed, neither the vacuolation nor the nuclear phenotypes showed any interpretable correlation with the incomplete penetrance summarized in Figure 2B. Consequently, it was not possible to use cytological criteria to order the six *spe-5* mutations into an allelic series.

Organelle and macromolecular segregation in *spe-5*: *spe-5* mutants appear to have defects in the proper segregation of nuclei and cytoplasm during division. Previous studies of spermatogenesis have identified several proteins (tubulin, actin and MSP) and organelles (nuclei, ribosomes and FB-MOs) that are nonrandomly segregated during the asymmetrical second meiotic division of spermatogenesis (ROBERTS *et al.* 1986; WARD 1986). Phalloidin, which binds with high specificity to F-actin, and antibodies that recognize tubulin, MSP and an antigen that is specifically localized within MOs were employed. Each of these four reagents binds to a different protein that is asymmetrically partitioned during spermatid formation, and they were employed in immunofluorescence experiments to characterize *spe-5* mutants. Figure 5, A–L shows a summary of these segregation phenotypes in *dpy-5(e61); him-5(e1490)* control sperm. For each cell, a DIC image is shown (Figure 5, A–D, followed by the DAPI-stained image to visualize the nuclei (Figure 5, E–H), and then the immunofluorescence image for the indicated antigen (Figure 5, I–L). Phalloidin staining indicates that the majority of the F-actin resides in the residual body (RB) after the second meiotic division (Figure 5I), whereas the nuclei are in the budding spermatids (Figure 5, A and E). Tubulin follows the same pattern as actin and partitions to the RB (Figure 5J) and away from the nuclei in the buds (Figure 5, B and F). Note the intense tubulin staining at the spindle poles (yellow dots in the residual body, Figure 5J). In contrast, the 1CB4 antigen (Figure 5K) and MSP (Figure 5L) segregate to the budding spermatids with the nuclei. Both 1CB4 (Figure 5K) and MSP (Figure 5L) staining appears somewhat punctate, reflecting the vesicular nature of the FB-MOs.

Cytoplasmic segregation in *spe-5* mutants is difficult to assess because spermatocytes usually arrest without attempting to form spermatids. Nevertheless, all *spe-5* mutant alleles are incompletely penetrant, so each mutant occasionally produces spermatocytes that initiate the budding stage. Actin segregation appears normal in such *spe-5* mutant cells. Phalloidin staining is confined to the RB and is absent or reduced in spermatids (Figure 5, M, R and W). MO and MSP segregation is also normal in *spe-5* cells that progress to the budding stage. The MOs are visualized by 1CB4 staining (Figure 5Y), partition with nuclei (Figure 5T) to the budding spermatids (Figure 5O) and appear punctate as in wild-type cells (Figure 5K). The anti-MSP staining (Figure 5Z) is also confined to spermatids (Figure 5P) where the nuclei reside (Figure 5U). In contrast, tubulin segregation appears disrupted in a *spe-5* background. Tubulin staining is concentrated at the sites of budding and diffuses into the budding spermatids (Figure 5X), where the nuclei segregate (Figure 5S). However, this tubulin mis-segregation phenotype is not completely penetrant. In some instances, tubulin segregates properly to the RB as in the cell shown in Figure 5BB. This is the same cell as Figure 5M and it has been stained for both actin (Figure 5W) and tubulin (Figure 5BB). Another variation on the phenotypes presented above is that the nuclei do not always segregate to bud-like structures (Figure 5, Q and V). When nuclei fail to segregate to developing spermatids, MSP is diffusely scattered throughout the cell with no clear segregation pattern (Figure 5AA); this is also true for tubulin, actin, and the 1CB4 antigen (data not shown).

***spe-5* ultrastructural phenotype:** Light microscopic

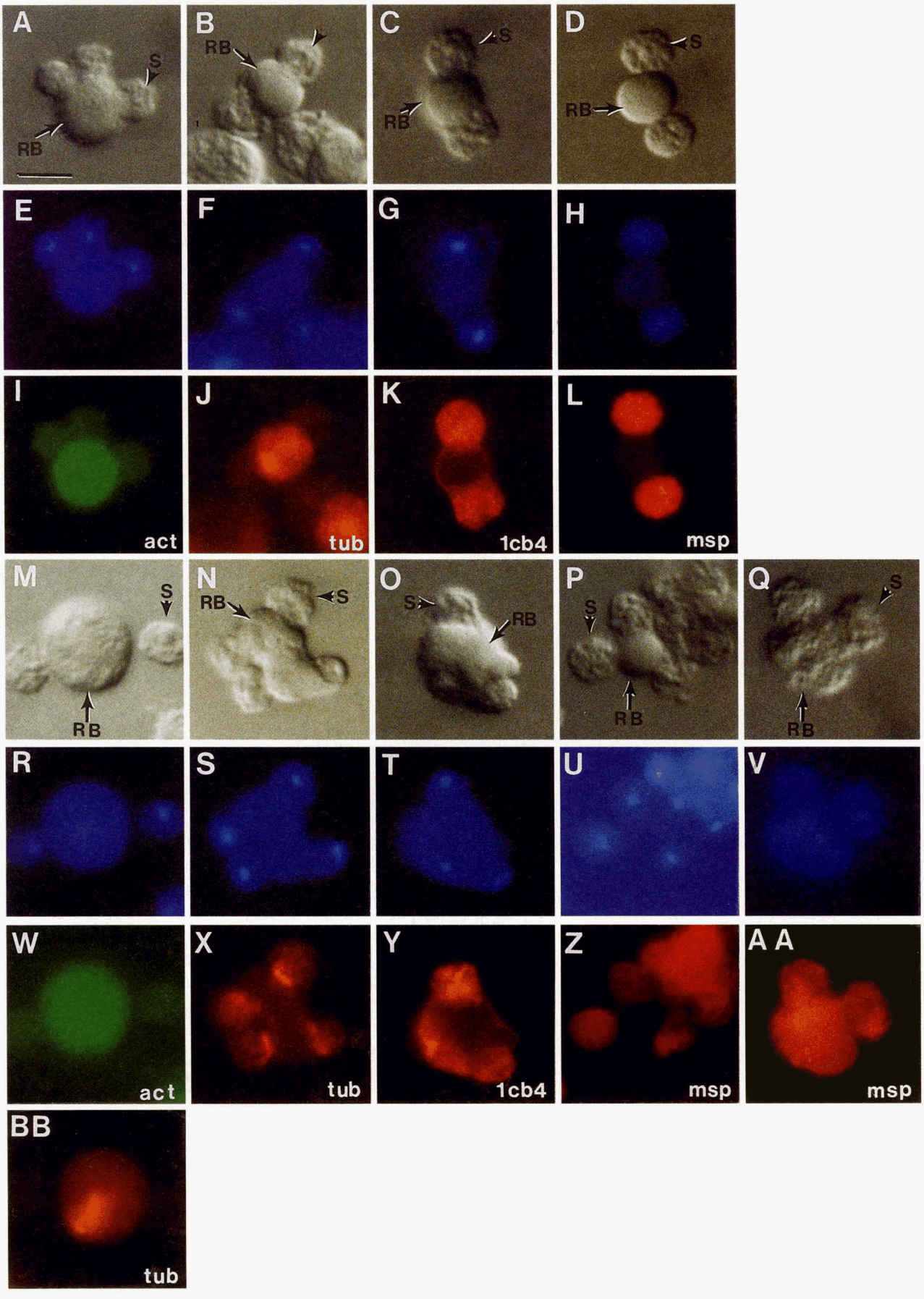
A
S
RB
B
RB
C
S
RB
D
S
RB
E
F
G
H
I
act
J
tub
K
1cb4
L
msp
M
S
RB
N
RB
S
O
S
RB
P
S
RB
Q
S
RB
R
S
T
U
V
W
act
X
tub
Y
1cb4
Z
msp
A A
msp
BB
tub

analyses revealed FB-MO defects in *spe-5* mutant sperm. We performed an ultrastructural analysis of spermatogenesis in *spe-5* mutants to further examine these *spe-5* FB-MO differentiation defects at higher resolution (Figures 6 and 7). A summary of wild-type and *spe-5* mutant FB-MO ultrastructural morphogenesis appears in Figure 8. The earliest observable phenotype in *spe-5* cells appears when spermatocytes are still in a syncytium with the rachis. At this stage, small vacuoles are present throughout the cytoplasm of *spe-5* spermatocytes (Figure 6D). In contrast, wild-type cells at the same stage of differentiation have several maturing FB-MOs scattered throughout the cytoplasm, and the vacuoles observed in *spe-5* cells are absent (Figure 6A). The uncondensed nature of the nuclei in these cells indicates that they are primary spermatocytes. Aberrant FB-MO structures appear in *spe-5* primary spermatocytes (Figure 6E). The close association of the double layered membrane surrounding the FB in wild-type FB-MOs (Figures 6A and 8Ab) is disrupted in *spe-5* cells (Figures 6E and 8Bb and c). The two membranes surrounding the FB are separated by a large vacuolar space, which is probably responsible for the prominent, cratered appearance observed by light microscopy (Figures 4, I–M and 5, M–Q). This defect does not prevent association between the FB and MO, which remain closely connected. In addition to the large vacuoles that are associated with FBs, smaller vacuoles that are sometimes associated with FBs are also found throughout the cytoplasm (Figure 6, E and F). In wild type, the FB is exposed when the double layered membrane surrounding this structure is retracted during spermatid budding (Figure 6B). The membrane surrounding the FB is apparently folded up and retracted into the body of the MO during exposure of the wild-type FB (Figures 6B and 8Ac). The MSP polymers that compose the FB are then disassembled into their constituent dimers and no FB structures are visible in budded wild-type spermatids (Figure 6C). The FB is also exposed during *spe-5* FB-MO morphogenesis, but at an earlier time and in a fundamentally different way. In *spe-5* terminal spermatocytes, a swollen vacuolar space forms between the two membranes that surround the FB (Figure 6, E and F; Figure 8, Ba–c). Consequently, the FB is never properly surrounded by a double layered membrane (Figure 6, E and F; Figure 8, Ba–c) The synchrony between nuclear condensation, cell division, and FB-MO differentiation present in wild-type cells is also lost in *spe-5* mutant sperm. The MO vacuolation phenotype is seen before (Figure 6E) and after (Figure 6F; Figure 7B) nuclear condensation when *spe-5* cells are arrested as terminal spermatocytes. Defective FB-MOs are a penetrant aspect of the *spe-5* phenotype because normal FB-MOs were not observed in several EM preparations processed from hundreds of *spe-5* males.

Terminal spermatocytes containing defective FB-MOs are the most common cell type observed during spermatogenesis in *spe-5* mutants. However, all six *spe-5* mutations are incompletely penetrant and sometimes allow spermatids to form in either sex. A few cells that are attempting to divide and/or form spermatids have been characterized by EM and they also contain defective FB-MOs (Figure 7). *spe-5* mutant cells can initiate the first (Figure 7A) and second (Figure 7B) meiotic divisions, but many aspects of these processes appear abnormal. During the second division, condensed nuclei and mitochondria segregate to the budding spermatids, as in wild type, but FB-MOs seem to lag behind and remain scattered throughout the cell. Nonetheless, FB-MOs can segregate properly to the budding cells in those cases where spermatids form successfully. Such spermatids invariably have defective MOs (Figure 8C). Nonetheless, MSP polymer fibers can disassociate from MOs and depolymerize because intact FBs are not observed in *spe-5* budded spermatids. The nuclei in *spe-5* spermatids have a normal, highly condensed appearance, but MOs have an irregular, distended appearance when compared to wild type (Figure 7C). Furthermore, MOs do not always reside just below the plasma membrane in *spe-5* spermatids (Figure 7C) as is the case in wild type (Figure 6C). The density of internal MO membranes in *spe-5* spermatids tends to be lower than that observed for wild type. Disrupted MOs in *spe-5* spermatids can occasionally abut below the plasma membrane (Figure 7C), and can fuse with it to form a permanent fusion pore (Figure 7D) as is observed for a few MOs in wild-type spermatids (Figure 6C). The *spe-5* cytological and FB-MO defects are summarized in Figures 3B and 8B.

DISCUSSION

The *spe-5* gene is presently defined by a total of six alleles. Two of these alleles were recovered as false posi-

FIGURE 5.—Segregation of tubulin, actin, MSP and fibrous body-membranous organelle complexes (FB-MOs). Dividing spermatocytes at the budding spermatid stage were obtained from *dpy-5(e61); him-5(e1490)* males (A–L) or *spe-5(hc110)dpy-5(e61); him-5(e1490)* (M–BB). DIC images are shown in first row for wild type (A–D) and the fourth row for *spe-5* (M–Q). The same cells imaged by DIC were also stained with DAPI (E–H for wild type; R–V for *spe-5*) to visualize their nuclei and various reagents to reveal the distribution of specific proteins within sperm (I–L for wild type; W–BB for *spe-5*). Specific proteins visualized were as follows: actin (act), tubulin (tub), an antigen (recognized by monoclonal antibody 1CB4) that is specific for the membranous organelle portion of the FB-MO or the major sperm protein (msp), which composes the fibrous body portion of the FB-MO. See MATERIALS AND METHODS for details on the antibodies and other reagents used to visualize specific proteins within sperm. Males with the above indicated genotype were picked as L4 virgins and aged for 2–4 days at 16° before dissection to release sperm for cytological analyses. RB refers to residual body, and S to spermatid. Scale bar in A = 5 μm for A–BB.

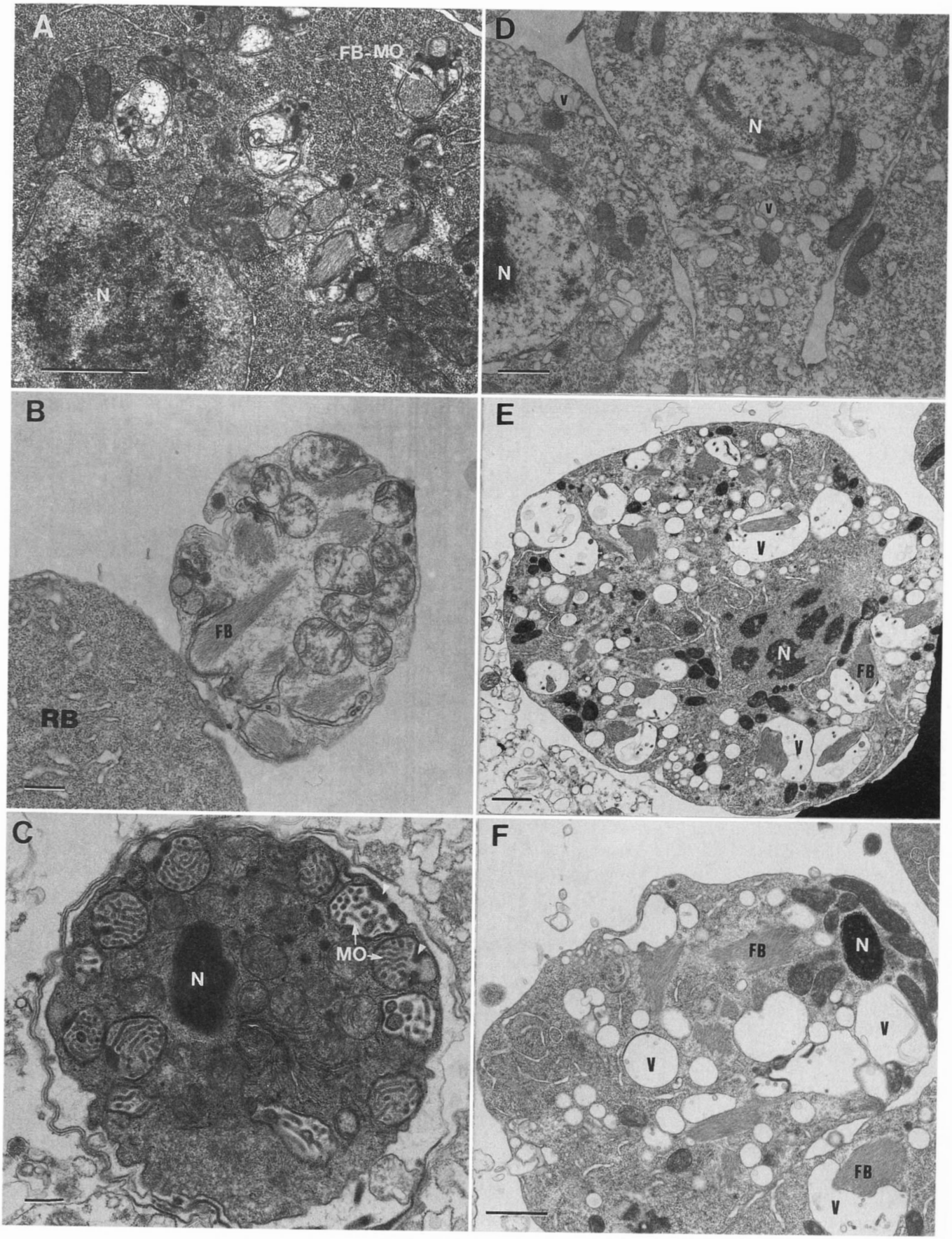
A
FB-MO
N
D
V
N
V
N
B
FB
RB
E
V
N
FB
V
C
MO
N
F
FB
N
V
V
FB
V

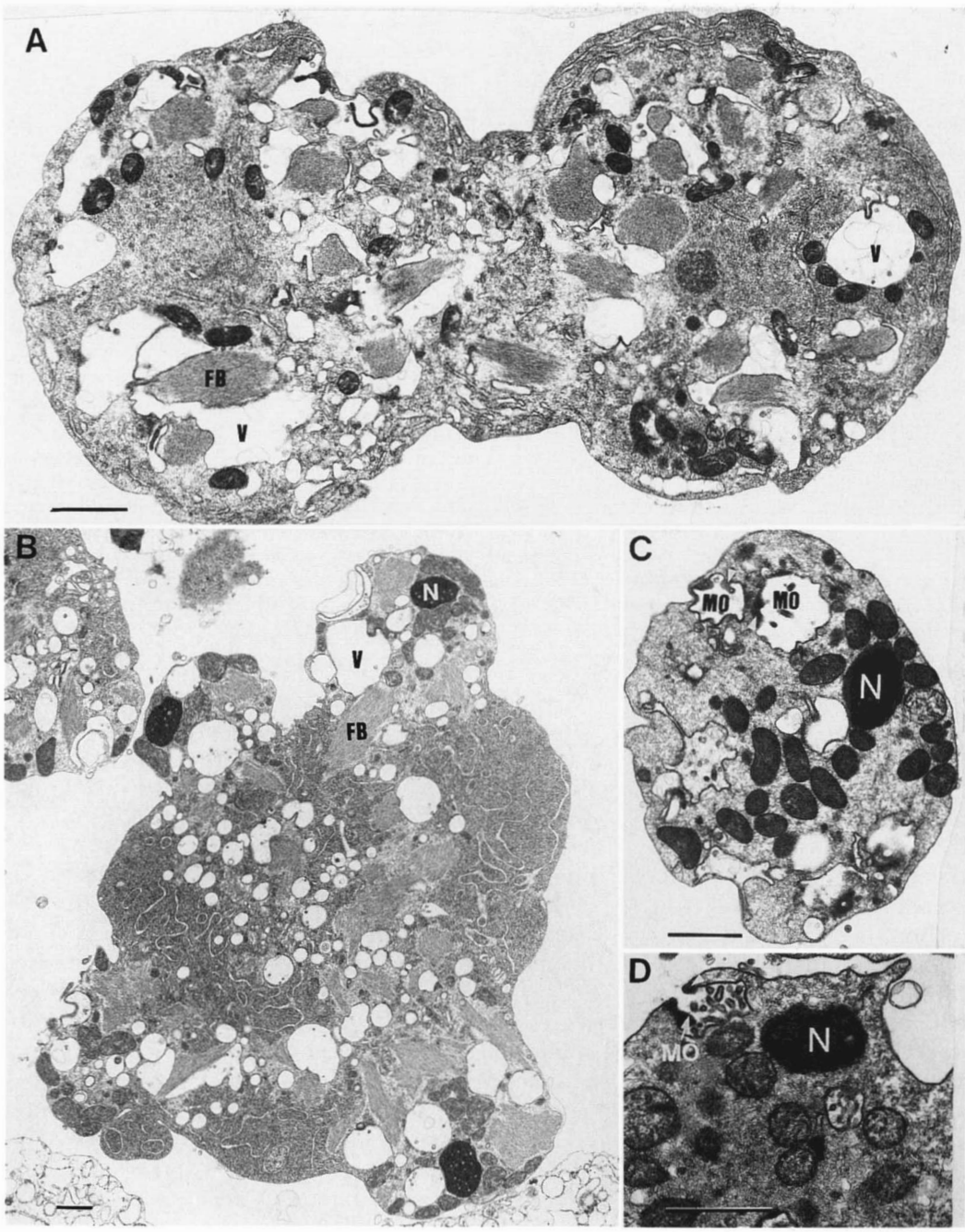

FIGURE 7.—*spe-5* FB-MO morphogenesis. Cells were obtained from *spe-5(hc110) dpy-5(e61); him-5(e1490)* males that have been picked as L4s and aged for 3 days at 20° (A, C and D) or 16° (B). (A) A primary spermatocyte undergoing the first meiotic division. (B) A spermatocyte at the spermatid budding stage. (C) A spermatid. (D) A fused membranous organelle (MO) in a spermatid. All scale bars are 1 μm. FB, fibrous body; V, vacuole; N, nucleus. The collar regions of MOs are indicated with white arrow heads in C and D.

tives in a F_2 genome wide screen for females, and the number of chromosomes sampled was not recorded (T. SCHEDL, personal communication). Two alleles were recovered in a F_2 screen for chromosome I *spe* genes that sampled 3838 chromosomes (L'HERNAULT *et al.* 1988), while the last two were recovered in an F_1 screen

FIGURE 6.—*spe-5* ultrastructural phenotype. (A–C) Cells from *dpy-5(e61); him-5(e1490)* males showing the sequential development of fibrous body-membranous organelle complexes (FB-MOs) in the control genetic background. (A) Cellular morphology in primary spermatocytes attached to the rachis. (B) A spermatid that has almost completed budding. (C) A spermatid that is just initiating its development into a spermatozoan. The FB-MOs are a prominent feature of spermatocytes (A) and budding spermatids (B). The disassembling FB evident in B results in a MO, and these MOs fuse with the plasma membrane (arrowheads in C) as spermatids initiate pseudopodial extension and become spermatozoa. (D–F) Cells from *spe-5(hc110) dpy-5(e61); him-5(e1490)* males and show the various defects observed in a *spe-5* mutant background. (D) The cellular morphology of primary spermatocytes attached to the rachis. (E) A defective primary spermatocyte with an uncondensed nucleus (N). (F) A terminal-stage spermatocyte with a condensed nucleus. All cells are from males that were isolated as L4 virgins and aged for 3 days at 16°. Normal-appearing FB-MOs were never observed in *spe-5* mutants at any developmental stage. FB, fibrous body; MO, membranous organelle; RB, residual body; N, nucleus; V, vacuole. The white arrow heads indicate the collar region of the FB-MO complex. Bars, 1 μm.

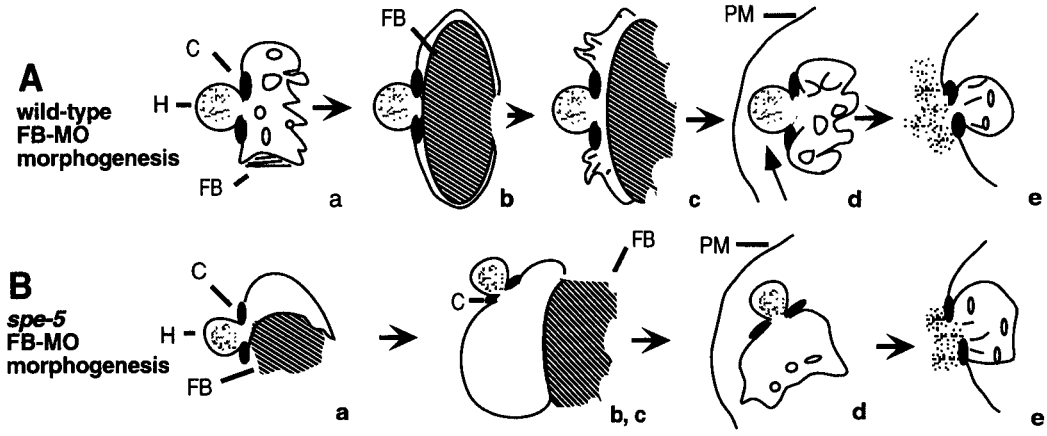

FIGURE 8.—Cartoon summary of fibrous body-membranous organelle (FB-MO) morphogenesis in wild-type animals (A) and the observed ultrastructural defects in *spe-5* mutants (B). For both wild-type and *spe-5* cells, the fibrous body (FB) develops in association with the membranous organelle (MO), and these two structures are separated by an electron-dense collar (C). In wild-type, stages a and b are found in spermatocytes, stage c in budding spermatids, stage d in budded spermatids and stage e in spermatozoa. There is no clear distinction between stages b and c during *spe-5* spermatogenesis. In most cases, spermatogenesis in *spe-5* mutants arrests at stage b, c in spermatocytes that do not subsequently form spermatids. Occasionally, spermatids (Bd) and spermatozoa (Be) form in *spe-5* mutants. Note that the FB in *spe-5* cells is never partially surrounded by membranes of the MO as it is in wild-type cells, and a large vacuole forms (open oval in Bb, c). Each cell has many FB-MO complexes. PM, plasma membrane. For further explanation, see the text.

of 7324 chromosomes. The recovery of four mutations out of 11,162 screened chromosomes yields a forward mutation rate for *spe-5* of 3.6×10^{-4}, which is lower than the 5×10^{-4} knockout rate for an average *C. elegans* gene (BRENNER 1974). Possibly, *spe-5* might be a small EMS mutational target due either to unusual DNA base composition or small gene size. All *spe-5* mutant hunts were performed at 25° to search for temperature-sensitive alleles. The tendency of *spe-5* mutations to exhibit incomplete penetrance for the self-sterile phenotype, especially at the 25° growth temperature, could have resulted in mutants that were not scorable as Spe. Alternatively, this collection of *spe-5* alleles might be a biased set that does not include null mutations. The fact that *spe-5(hc110)* homozygotes and *spe-5(hc110)/sDf4* hemizygotes are both Spe and phenotypically indistinguishable suggests that the null phenotype of *spe-5* is Spe and not a more severe germline/gonad defect or lethality. It also indicates that F_1 noncomplementation screens should permit recovery of any type of mutation, including deficiencies, that fail to complement *spe-5*. The two mutations recovered in the noncomplementation screen described in this paper were both Spe, suggesting that this is the null phenotype.

The earliest detectable cytological defect in *spe-5* mutants is a dramatic vacuolation of the spermatocyte cytoplasm due to distended FB-MOs. These organelles play a major role in the segregation of molecular components to spermatids during their budding from the residual body (reviewed by L'HERNAULT 1997). While terminal spermatocytes are a common end point of spermatogenesis in *spe-5* mutants, spermatid budding is also observed and macromolecular partitioning can be assessed in such cells. The defective FB-MOs observed in *spe-5* mutants might be associated with or, perhaps, cause generalized defects in the asymmetric macromolecular segregation that occurs during spermatid budding. Usually, this was not the case because FB-MOs (as detected with the anti-MO 1CB4 or anti-MSP antibodies) and actin could asymmetrically partition to *spe-5* mutant spermatids and residual bodies, respectively, as it does in wild type during budding (Figure 5). The segregation of tubulin is variable in *spe-5* mutants, and it sometimes missegregates to spermatids while, in other cells, it partitions to the RB like wild type. The proper segregation of actin and FB-MOs coupled with an incompletely penetrant tubulin mis-segregation phenotype suggest that *spe-5* mutant sperm do not have a general macromolecular partitioning defect. The precise mechanism by which FB-MOs are segregated to wild-type spermatids in *C. elegans* is unknown. In the parasitic nematode Ascaris, MOs are known to be associated with the meiotic spindle poles during meiosis II (T. ROBERTS, personal communication), and this association might also occur during *C. elegans* spermatogenesis. Perhaps, *spe-5* mutants have defects that cause FB-MOs to stay inappropriately associated with the meiotic spindle. Consequently, the meiotic spindle would be passively segregated into spermatids due to this association, since FB-MO segregation to *spe-5* spermatids can occur. If this hypothesis is true, it would also explain the unusual tubulin morphology observed in *spe-5* terminal spermatocytes, where tubulin staining occasionally appears as clumps that co-localizes with the nuclei (data not shown).

Phenotypic analyses clearly indicates that *spe-5* is required for FB-MO morphogenesis. Nevertheless, despite prominent FB-MO defects, some *spe-5* mutant cells

can undergo all steps required for spermatids formation, including division, intracellular segregation, bud formation, release of spermatids from the residual body and spermatid activation into spermatozoa. Consequently, the machinery for these processes can function in *spe-5* mutant cells, but coordination between various steps appears poor. The six *spe-5* mutants and hemizygous *spe-5(hc110)*/deficiency hermaphrodites all show incomplete penetrance for self-sterility (Figure 2). This indicates that functional spermatozoa are formed in all *spe-5* mutants and suggests that either none of them is null or there is not an absolute requirement for *spe-5* during spermatogenesis.

A number of other spermatogenesis defective mutants that affect FB-MO morphogenesis in *C. elegans* have been characterized. Among this collection, *spe-4* mutants appear to have FB-MO and other phenotypic defects that are similar to those observed in *spe-5* mutants (L'HERNAULT *et al.* 1988; L'HERNAULT and ARDUENGO 1992). The SPE-4 protein is localized within FB-MOs during spermatogenesis, indicating that all aspects of the *spe-4* mutant phenotype result from a lack of this protein within these organelles (P. M. ARDUENGO, P. CHUANG, O. K. APPLEBERRY and S. W. L'HERNAULT, unpublished data). Both *spe-4* and *spe-5* mutants contain spermatocytes with disrupted FB-MOs and vacuolation of the cytoplasm, but these defects appear much more pronounced in *spe-5* animals. Surprisingly, *spe-4* null mutants are completely self-sterile and are never observed to produce spermatids or spermatozoa. The complete penetrance of self-sterility exhibited by *spe-4* null mutants indicates that proper FB-MO morphogenesis is required for spermatid formation. The formation of spermatids and spermatozoa by *spe-5* mutants shows that these cells can still form even when FB-MO morphogenesis is profoundly disrupted. In principle, the spermatozoa responsible for the weak self-fertility exhibited by *spe-5* mutants might result from cells in which proper FB-MO morphogenesis occurred. However, this seems unlikely because all observed *spe-5* spermatids and spermatozoa contained defective FB-MOs. This suggests that *spe-5* has a partly dispensable role in coordinating the proper formation of spermatids, and that an occasional *spe-5* spermatid can form a functional spermatozoon, in spite of abnormal FB-MO morphogenesis.

Several *spe/fer* mutations also uncouple cellular formation and maturation from FB-MO morphogenesis during spermatogenesis. *fer-1* spermatids contain MOs that fail to fuse with the plasma membrane during the activation process that converts them into spermatozoa. Although MO fusion with the plasma membrane occurs before pseudopod extension in wild-type, *fer-1* mutant spermatids can extend a pseudopod in its absence. Defects in MO fusion with the plasma membrane are also observed in *spe-10* mutants. In *spe-10* mutants, FBs are discarded in the residual body, but the MOs can still segregate into spermatids and rarely fuse with the plasma membrane (SHAKES and WARD 1989). However, the pseudopod present on both *spe-10* and *fer-1* spermatozoa is shorter than wild type (WARD *et al.* 1981), *fer-1* or *spe-10* spermatozoa cannot properly crawl *in vitro* (WARD and CARREL 1979) and strong loss of function mutants are almost completely self-sterile (L'HERNAULT *et al.* 1988; SHAKES and WARD 1989). *spe-17* null mutants contain FB-MOs that, unlike wild type, have membrane-bound ribosomes (SHAKES and WARD 1989). FB-MOs are properly segregated into *spe-17* spermatids during their budding from the residual body, and these abnormally small spermatids can activate into spermatozoa (SHAKES and WARD 1989; L'HERNAULT *et al.* 1993). Resulting *spe-17* spermatozoa all have short pseudopods, but this does not prevent a few of them from crawling and successfully fertilizing oocytes (SHAKES and WARD 1989; L'HERNAULT *et al.* 1993). As for *spe-5,* there is no evidence that *spe-17* null mutants ever produce spermatozoa with completely normal cytology. Since *spe-17* null mutants are deletions that completely remove the gene, the weak self-fertility of these mutants cannot be due to residual gene function. Rather, *spe-17* function is not essential for producing spermatozoa that can successfully fertilize oocytes, which is perhaps also the case for *spe-5* mutants.

In addition to *spe-5* males, other spermatogenesis-defective mutants that exhibit early spermatogenesis arrest, like *spe-4* (L'HERNAULT *et al.* 1988) and *spe-6* (VARKEY *et al.* 1993), produce fewer sperm cells than wild-type or control males. This could be due to attenuated spermatogenesis, or, alternatively, *spe-5* mutant males could be producing normal numbers of cells that cannot maintain their cellular integrity for extended periods of time, and eventually die and are resorbed. Perhaps, the low spermatocyte number in *spe-5* is due to feedback regulation of the number of primary spermatocytes present at a given time.

Certain alleles of many genes in *C. elegans* exhibit a conditional phenotype that is affected by growth temperature. Commonly, mutations will be temperature-sensitive so that a mutant phenotype is only evident at one temperature that is higher than the permissive temperature, where the phenotype is either less evident or not detectable. Less commonly, a process itself is intrinsically temperature-sensitive, and the most thoroughly studied example in *C. elegans* is the dauer formation pathway (GOLDEN and RIDDLE 1984). Several genes in the dauer formation pathway are defined only by temperature-sensitive alleles, and these include nonsense mutations. This suggests that dauer formation is a process that is intrinsically temperature-sensitive.

All six *spe-5* mutants exhibit cold sensitivity (cs) (Figure 2). Cold sensitivity is rare in *C. elegans,* but it has been reported for several genes (HOSONO 1980; HARTMAN and HERMAN 1982; WU and HAN 1994; AHRINGER 1995). Cold sensitivity is usually specific for particular

mutations and is observed in a variety of processes including embryonic tissue differentiation (AHRINGER 1995), radiation sensitivity (HARTMAN and HERMAN 1982), external morphology (HOSONO 1980), and vulval differentiation (WU and HAN 1994). Since the observed cs phenotypes are usually allele specific, they are presumably due to mutations that alter the protein conformation so it becomes functionally cs. Protein structure is dependent on hydrophobic interactions that are weakened at lower temperature (BALDWIN 1986) and could be associated with a cs phenotype. cs mutations have also been identified in several other organisms ranging from *Escherichia coli* (GINES-CANDELARIA *et al.* 1995) to mammals (ZIMMERMAN *et al.* 1983), and are involved in a variety of cellular processes including protein secretion (POGLIANO and BECKWITH 1993), ribosome assembly (FALKE and WRIGHT 1975) and nuclear division (MOIR and BOTSTEIN 1982). In most instances the cs mutations appear to be exceptional in an allelic series, except for the protein secretion pathway in *E. coli* (POGLIANO and BECKWITH 1993). Most of the mutant alleles in four *E. coli* genes (*sec*D, *sec*E, *sec*F, and *sec*Y) involved in protein export are cold-sensitive. Furthermore, regulatory mutations that simply lower the amount of wild-type SecE protein result in a protein export pathway that is cs. This argues that the protein export pathway in *E. coli* has an inherent cold-sensitive step (POGLIANO and BECKWITH 1993).

In addition to the *spe-5*-associated cold-sensitivity, *spe-4* mutations also exhibit a cs oocyte laying phenotype, and this includes a null allele that partly deletes the gene (P. M. ARDUENGO and S. L'HERNAULT, unpublished data). Both *spe-4* and *spe-5* exhibit defective FB-MO morphogenesis. It seems unlikely that six independently isolated *spe-5* mutations and two examined, independent *spe-4* mutations result is conformational changes in both proteins that lead to the observed cs phenotypes. Perhaps a more probable explanation is that *spe-5* and *spe-4* mutants reveal that FB-MO morphogenesis is an inherently cold-sensitive process.

The authors thank NANCY L'HERNAULT for assistance with electron microscopy. We also thank Drs. TIM SCHEDL and P. MICHELE ARDUENGO for *spe-5* alleles, Drs. WINFIELD SALE, SAMUEL WARD, JULIE AHRINGER and JONATHAN HODGKIN for providing us with antibodies and CRAIG HEILMAN and Dr. ALLAN I. LEVEY for preparation of the hybridoma supernatant from the monoclonal line 1CB4. Special thanks go to the L'HERNAULT lab members for advice and discussions and to HILARY ELLIS, JOHN LUCCHESI, BARRY YEDVOBNICK, HARISH JOSHI and two anonymous reviewers for careful critiques of the manuscript. The Caenorhabditis Genetic Center provided some nematode strains, and it is funded by the National Institutes of Health National Center for Research Resources. This work was supported by a grant from the Emory University Research Committee and U.S. Public Health Service grant GM-40697 to S.W.L.

LITERATURE CITED

ADACHI, Y., T. TODA, O. NIWA and M. YANAGIDA, 1985 Differential expressions of essential and nonessential alpha-tubulin genes in *Schizosaccharomyces pombe*. Mol. Cell Biol. **6:** 2168–2178.

AHRINGER, J., 1995 Embryonic tissue differentiation in *Caenorhabditis elegans* requires *dif-1*, a gene homologous to mitochondrial solute carriers. EMBO J. **14:** 2307–2316.

BALDWIN, R. L., 1986 Temperature dependence of the hydrophobic interaction in protein folding. Proc. Natl. Acad. Sci. USA. **83:** 8069–8072.

BAZINET, C., R. VILLAFANE and J. KING, 1990 Novel second-site suppression of a cold-sensitive defect in phage P22 procapsid assembly. J. Mol. Biol. **216:** 701–716.

BOOHER, R., and D. BEACH, 1987 Interaction between cdc13+ and cdc2+ in the control of mitosis in fission yeast; dissociation of the G1 and G2 roles of the cdc2+ protein kinase. EMBO J. **6:** 3441–3447.

BRENNER, S., 1974 The genetics of *Caenorhabditis elegans*. Genetics **77:** 71–94.

BURKE D. J., and S. WARD, 1983 Identification of a large multigene family encoding the major sperm protein of *Caenorhabditis elegans*. J. Mol. Biol. **171:** 1–29.

COLLINS, J., B. SAARI and P. ANDERSON, 1987 Activation of a transposable element in the germ line but not the soma of *C. elegans*. Nature **328:** 726–728.

DRUBIN, D. G., 1991 Development of cell polarity in budding yeast. Cell **65:** 1093–1096.

EATON, S., and K. SIMONS, 1995 Apical, basal and lateral cues for epithelial polarization. Cell **82:** 5–8.

FALKE, E. V., and T. R. WRIGHT, 1975 Cold-sensitive mutants of *Drosophila melanogaster* defective in ribosome assembly. Genetics **81:** 655–682.

FANE, B. A., and M. HAYASHI, 1991 Second-site suppressors of a cold-sensitive prohead accessory protein of bacteriophage phi X174. Genetics **128:** 663–671.

GINES-CANDELARIA, E., A. BLINKOVA and J. R. WALKER, 1995 Mutations in *Escherichia coli* dnaA which suppress a dnaX(Ts) polymerization mutation and are dominant when located in the chromosomal allele and recessive on plasmids. J. Bacteriol. **177:** 705–715.

GOLDEN, J. W., and D. L. RIDDLE, 1984 A pheromone-induced developmental switch in *Caenorhabditis elegans:* temperature-sensitive mutants reveal a wild-type temperature-dependent process. Proc. Natl. Acad. Sci. USA **81:** 819–823.

HARTMAN, P. S., and R. K. HERMAN, 1982 Radiation-sensitive mutants of *C. elegans*. Genetics **102:** 159–178.

HIRSH, D., D. OPPENHEIM and M. KLASS, 1976 Development of the reproductive system of *Caenorhabditis elegans*. Dev. Biol. **49:** 200–219.

HODGKIN, J., H. R. HORVITZ and S. BRENNER, 1979 Nondisjunction mutants of the nematode *Caenorhabditis elegans*. Genetics **91:** 67–94.

HOSONO, R., 1980 A study of morphology of *C. elegans:* a mutant of *C. elegans* with dumpy and temperature-sensitive roller phenotype. J. Exp. Zool. **213:** 61–67.

HOWELL, A. M., S . G. GILMOUR, R. A. MANCEBO and A. M. ROSE, 1987 Genetic analysis of a large autosomal region in *C. elegans* by the use of a free duplication. Genet. Res. **49:** 207–213.

HSIAO, C. L., and L. W. BLACK, 1977 DNA packaging and the pathway of bacteriophage T4 head assembly. Proc. Natl. Acad. Sci. USA **74:** 3652–3656.

KIMURA, Y., S. MATSUMOTO and I. YAHARA, 1994 Temperature-sensitive mutants of hsp82 of the budding yeast *Saccharomyces cerevisiae*. Mol. Gen. Genet. **242:** 517–527.

KLASS, M., N. WOLF and D. HIRSH, 1976 Development of the male reproductive system and sexual transformation in the nematode *Caenorhabditis elegans*. Dev. Biol. **52:** 1-18.

KLASS, M. R., and D. HIRSH, 1981 Sperm isolation and biochemical analysis of the major sperm protein from *Caenorhabditis elegans*. Dev. Biol. **84:** 299–312.

L'HERNAULT, S. W., 1997 Male germline, in *C. elegans II,* pp. 271–294 in edited by D. RIDDLE, T. BLUMENTHAL, B. J. MEYER and J. PRIESS. Cold Spring Harbor Laboratory Press, Cold Spring Harbor, NY.

L'HERNAULT, S. W., and P. M. ARDUENGO, 1992 Mutation of a putative sperm membrane protein in *Caenorhabditis elegans* prevents sperm differentiation but not its associated meiotic divisions. J. Cell Biol. **119:** 55–68.

L'HERNAULT, S. W., D. C. SHAKES and S. WARD, 1988 Developmental

genetics of chromosome I spermatogenesis-defective mutants in the nematode *Caenorhabditis elegans*. Genetics **120:** 435–452.

L'HERNAULT, S. W., G. M. BENIAN and R. B. EMMONS, 1993 Genetic and molecular characterization of the *Caenorhabditis elegans* spermatogenesis-defective gene *spe-17*. Genetics **134:** 769–780.

LEVY-LAHAD, E., W. WASCO, P. POORKAJ, D. M. ROMANO, J. OSHIMA *et al.*, 1995 Candidate gene for the chromosome 1 familial Alzheimer's disease locus. Science **269:** 973–977.

LEWIS, J. A., C. H. WU, H. BERG and J. H. LEVINE, 1980 The genetics of levamisole resistance in the nematode *C. elegans*. Genetics **95:** 905–928.

MACHACA, K., L. J. DEFELICE and S. W. L'HERNAULT, 1996 A novel chloride channel localizes to *Caenorhabditis elegans* spermatids and chloride channel blockers induce spermatid differentiation. Dev. Biol. **176:** 1–16.

MCKIM, K. S., and A. M. ROSE, 1990 Chromosome I duplications in *Caenorhabditis elegans*. Genetics **124:** 115–132.

MOIR, D., and D. BOTSTEIN, 1982 Determination of the order of gene function in the yeast nuclear division pathway using cs and ts mutants. Genetics **100:** 565–577.

MOSTOV, K. E., and M. H. CARDONE, 1995 Regulation of protein traffic in polarized epithelial cells. Bioessays **17:** 129–138.

NABESHIMA, K., H. KUROOKA, M. TAKEUCHI, K. KINOSHITA, Y. NAKASEKO *et al.*, 1995 p93dis1, which is required for sister chromatid separation, is a novel microtubule and spindle pole body-associating protein phosphorylated at the Cdc2 target sites. Genes Dev. **9:** 1572–85.

NELSON, G. A., T. M. ROBERTS and S. WARD, 1982 *C. elegans* spermatozoan locomotion: amoeboid movement with almost no actin. J. Cell Biol. **92:** 121–131.

OAKLEY, B. R., C. E. OAKLEY, K. S. KNIEPKAMP and J. E. RINEHART, 1985 Isolation and characterization of cold-sensitive mutations at the benA, beta-tubulin, locus of *Aspergillus nidulans*. Mol. Gen. Genet. **201:** 56–64.

OKAMOTO, H., and J. N. THOMSON, 1985 Monoclonal antibodies which distinguish certain classes of neuronal and supporting cells in the nervous tissue of the nematode *Caenorhabditis elegans*. J. Neurosci. **5:** 643–653.

PAULSEN, J. E., E. E. CAPOWSKI and S. STROME, 1995 Phenotypic and molecular analysis of *mes-3*, a maternal-effect gene required for proliferation and viability of the germ line in *C. elegans*. Genetics **141:** 1383–1398.

POGLIANO, K. J., and J. BECKWITH, 1993 The Cs sec mutants of *Escherichia coli* reflect the cold sensitivity of protein export itself. Genetics **133:** 763–773.

ROBERTS, T. M., and S. WARD, 1982 Membrane flow during nematode spermiogenesis. J. Cell Biol. **92:** 113–120.

ROBERTS, T. M., F. M. PAVALKO and S. WARD, 1986 Membrane and cytoplasmic proteins are transported in the same organelle complex during nematode spermatogenesis. J. Cell Biol. **102:** 1787–1796.

ROGAEV, E. I., R. SHERRINGTON, E. A. ROGAEVA, G. LEVESQUE, M. IKEDA *et al.*, 1995 Familial Alzheimer's disease in kindreds with missense mutations in a gene on chromosome 1 related to the Alzheimer's disease type 3 gene. Nature **376:** 775–778.

ROSE, A. M., 1980 Genetic studies of the gene coding for paramyosin in *Caenorhabditis elegans*; *unc-15* and the adjacent region, Ph.D. thesis, Simon Fraser University, Burnaby, B.C., Canada.

ROSE, A. M., D. L. BAILLIE and J. CURREN, 1984 Meiotic pairing behavior of two free duplications of linkage group I in *Caenorhabditis elegans*. Mol. Gen. Genet. **195:** 52-56.

SALE, W. S., J. C. BESHARSE and G. PIPERNO, 1988 Distribution of acetylated α-tubulin in retina and in *in vitro*-assembled microtubules. Cell Motil. Cytoskel. **9:** 243–253.

SHAKES, D. C., and S. WARD, 1989 Mutations that disrupt the morphogenesis and localization of a sperm-specific organelle in *Caenorhabditis elegans*. Dev. Biol. **134:** 307–316.

SHERRINGTON, R., E. I. ROGAEV, Y. LIANG, E. A. ROGAEVA, G. LEVESQUE *et al.*, 1995 Cloning of a gene bearing mis-sense mutations in early-onset familial Alzheimer's disease. Nature **375:** 754–760.

VARKEY, J. P., P. L. JANSMA, A. N. MINNITI and S. WARD, 1993 The *Caenorhabditis elegans spe-6* gene is required for major sperm protein assembly and shows second site non-complementation with an unlinked deficiency. Genetics **133:** 79–86.

WARD, S., 1986 Asymmetric localization of gene products during the development of *Caenorhabditis elegans* spermatozoa, pp. 55–75 in *Gametogenesis and the Early Embryo*, edited by J. G. GALL. Alan R. Liss, New York.

WARD, S., Y. ARGON and G. A. NELSON, 1981 Sperm morphogenesis in wild-type and fertilization defective mutants of *Caenorhabditis elegans*. J. Cell Biol. **91:** 26–44.

WARD, S., E. HOGAN and G. A. NELSON, 1983 The initiation of spermiogenesis in the nematode *Caenorhabditis elegans*. Dev. Biol. **98:** 70–79.

WOLF, N., D. HIRSH, and J. R. MCINTOSH, 1978 Spermatogenesis in males of the free living nematode, *Caenorhabditis elegans*. J. Ultrastruct. Res. **63:** 155–169.

WU, Y., and M. HAN, 1994 Suppression of activated Let-60 Ras protein defines a role of *Caenorhabditis elegans* Sur-1 MAP kinase in vulval differentiation. Genes Dev. **8:** 147–159.

ZIMMERMANN, A., J. C. SCHAER, D. E. MULLER, J. SCHNEIDER, N. M. MIODONSKI-MACULEWICZ *et al.*, 1983 Formation of mast cell granules in cell cycle mutants of an undifferentiated mastocytoma line: evidence for two different states of reversible proliferative quiescence. J. Cell Biol. **96:** 1756–1760.

Communicating editor: R. K. HERMAN